Vanadium Oxide -Titanium Oxide Nanocomposites for Enhanced Polymer Films

Ikram Mahdi Sabbar, Asaad Ahmed Kamil And Ammar Ayesh Habeeb
Department of Physics, College of Science, University of Diyala, 32001 Baqubah, Iraq
ikrammahdi65@gmail.com, Prof.asaad@uodiyala.edu.iq, ammarlaser72@yahoo.com

Keywords: Titanium Dioxide (TiO_2), Vanadium Dioxide (VO_2), Poly(Methyl Methacrylate) PMMA.

Abstract: The aim of this study is to prepare titanium oxide (TiO_2) using a sol–gel method and study its structural, optical, and morphological properties. These properties were then improved by mixing it with vanadium oxide (VO_2) to study the effect of the additive on the structure and energy gap. The TiO_2:VO_2 nanocomposite was then combined with polymethyl methacrylate (PMMA) to form a nanocomposite film. The properties of the TiO_2 nanocomposite were studied using FTIR analysis to determine the nature of the bonds and chemical interactions, and UV–Vis analysis to study the absorption and optical energy gap.The results showed that the prepared TiO_2 possesses an organized nanoscale anatase phase and good optical properties, while blending it with VO_2 resulted in a reduced energy gap and improved absorption in the visible range. The study of the PMMA–TiO_2: VO_2 composite membrane also revealed a clear interaction and homogeneity between the three components, resulting in improved structural and optical properties. These results demonstrate that the resulting composites possess promising properties for smart window and self-cleaning surface applications.

1 INTRODUCTION

Various organizations are conducting numerous research initiatives to develop and characterize polymer-nanoparticle composites, which are essential materials for modern technological applications [1], [2]. Notwithstanding their widespread applications, polymers are frequently acknowledged for their inferior mechanical strength and heat conductivity relative to metals and ceramics. Nonetheless, their advantages, such as being lightweight and cost-effective, render them attractive for numerous medical and engineering applications [3] Owing to its exceptional optical clarity, strong mechanical and thermal stability, appropriate dielectric properties, and chemical inertness, PMMA has become a preferred material in numerous manufacturing sectors, particularly in the optoelectronic industries [4]. Poly(methyl methacrylate) (PMMA) is widely recognized among polymers for its amorphous structure, linear polymer chains, and transparent characteristics. Its erosion resistance and endurance render it a reliable alternative to inorganic glass in numerous applications [5]. The distinct crystal phases of TiO_2 (anatase, rutile, and brookite) depend on the circumstances and preparation procedure of the sol-gel technology, which offers several advantages, including excellent homogeneity for the formation of high-quality nanostructures [6]. TiO_2 functions as an enhancement additive in polymer matrices, enhancing polymer structure and facilitating the optimization of nanocomposite films [7]. Because of their reversible temperature-dependent optical property changes, thermochromic materials have garnered a lot of attention recently. The most well-known thermochromic substance among them is vanadium dioxide VO_2, able to achieve a reversible insulator-to-metal transition (IMT) from an infrared-transparent semiconducting state to an infrared-reflective metallic state at room temperature about 68°C The intriguing characteristics of VO_2 render it appropriate for smart window applications [8], [9]. The formation of composites with polymers is a significant technique for enhancing the homogeneity of oxide nanoparticle-based films [10], [11]. Recent research indicate that VO_2/polymer composite films, produced with crystalline VO_2 nanoparticles, frequently encounter limitations in scalability and intricate processing, rendering them unsuitable for large-scale applications [12], [13].

2 MATERIALS AND METHODS

2.1 Materials

Titanium (IV) isopropoxide – 284.22 g/mol – Sigma-Aldrich – ≥97%, Hydrochloric acid (HCl) – 36.46 g/mol – ACS Chemicals, India – ≥99.5%,Ethanol C_2H_5OH – 46.07 g/mol – Sigma-Aldrich – ≥99.8%,Chloroform [$CHCl_3$]– 119.38 g/mol – ACS Chemicals, India – 99%, Poly(methyl methacrylate) (PMMA) $(C_5H_8O_2)_n$ – ~800,000 g/mol – A vonchem Ltd., UK, Vanadium oxide nano powder VO_2 – Hongwu International Group, China – 99.9%.

2.2 Preparation of TiO2 NPs

To produce TiO_2 nanoparticles, 300 mL of 70% ethanol was introduced into a beaker, Subsequently, 8 mL of titanium isopropoxide was added at room temperature. The solution was agitated with a magnetic stirrer for 60 minutes to achieve homogeneity. Subsequently, 40 mL of 0.1 M hydrochloric acid was introduced to the solution to modify the pH to roughly 4–5. The mixture was agitated for a further 60 minutes and thereafter subjected to sonication for 30 minutes. At this juncture, the solution had a milky look. he resulting suspension was centrifuged at 4200 rpm to separate the precipitate, Thereafter, it was rinsed four times with ethanol and deionized water. The obtained precipitate was dehydrated at 50°C for 48 hours. The dehydrated material was further calcined in a muffle furnace at 600°C for 2 hours to yield TiO_2 nanopowder.

2.3 Preparation of TiO2:VO2 NCs

To prepare TiO_2: VO_2 NPs with a VO_2 content of 5%, 0.095 g of TiO_2 was mixed with 0.005 g of VO_2 powder (This ratio was chosen with the aim of enhancing the surface properties without affecting the stability of the crystal structure and the homogeneity of the polymer film). The powder–powder mixing was carried out using a vortex mixer followed by mechanical stirring to ensure homogeneity.

2.4 Preparation of PMMA- TiO2:VO2 Thin-Film

0.5 g of PMMA was solubilized in 10 mL of $CHCl_3$ with continuous agitation for 2 hours. Followed by adding 30 mg of (TiO_2:VO_2)NCs and stirring for another 2 h in Figure 1, then ultrasonically dispersing the mixture for 20 min deposited on a glass slide (25.4 × 76.2 mm, thickness 1.2 mm) to dry at room temperature for 24h to form the PMMA - TiO_2;VO_2 nanocomposite thin film.

2.5 Characterization

The structural, morphological, and optical properties of the powder (TiO_2 NP_S, TiO_2:VO_2 NC_S) and PMMA - TiO_2;VO_2 thin film were characterized using the following techniques: XRD: AERIS benchtop diffractometer (Malvern Panalytical, Netherlands), Cu Kα radiation (λ = 1.54060 Å),
FTIR: Frontier FTIR spectrometer (PerkinElmer, USA), FESEM: Inspect™ F50 field emission scanning electron microscope (FEI Company), EDS: Integrated with Phenom desktop SEM (Thermo Fisher Scientific, Netherlands/USA), UV-Vis: Shimadzu UV-1900 spectrophotometer, wavelength range 200–1000 nm.

3 RESULTS AND DISCUSSION

3.1 X-Ray Diffraction Analysis Results

The structure of powder (TiO_2 NP_S and TiO_2:VO_2 NC_S) can be extensively analyzed using (XRD), a widely used method. This method may ascertain the crystal structure, lattice parameters, and crystallite dimensions of a substance [14]. Bragg's condition is satisfied when the x-rays are specularly reflected in a single atomic plane and constructively interfere with rays from successive atomic planes. Bragg's condition is expressed as follows [15]:

$$n\lambda\alpha = 2dhkl \sin\theta. \quad (1)$$

The number n signifies the diffraction order. λα denotes the wavelength of the incident x-ray. dhkl represents the interplanar distance. θ denotes Bragg's angle. The Sherri equation is shown in [15]:

$$D = k\,\lambda\alpha / \beta \cos\theta. \quad (2)$$

The shape factor is represented by k. λx the wavelength of the incident X-ray radiation is 1.5406 Å for CuKα. β denotes the full width at half maximum FWHM of the peak, expressed in radians. θ denotes Bragg's angle. An X-ray diffraction investigation was conducted to determine the structural phase of TiO_2. NP_S. The interplanar spacing (d) for the prepared materials was determined using Bragg's law based on the relationship.

Figure 2 illustrates the X-ray diffraction spectrum for TiO_2 nanoparticles, spanning the range of

approximately 20° to 80°. These results correspond with the ICDD card number 01-073-1764. The most pronounced peak occurs at the diffraction angle of 2θ=25.58°, with an average crystallite size (D) of 22.968 nm, which corresponds to the (101) crystal plane, a distinctive feature of the anatase phase, thereby confirming that the material is well-crystallized in this phase.

The crystal structure corresponding to these peaks is tetragonal [16], [17]. This is corroborated by the XRD data for TiO_2 nanoparticles, which are presented in Table 1 .Figure 2 displays the XRD patterns resulting from the physical mixing of TiO_2 and VO_2 nanoparticles. diffraction peaks can be indexed to the monoclinic phase of VO_2(M) (JCPDS card nos. 01-072-0514 and 01-073-1764) and correspond to VO_2 and TiO_2, respectively. no significant changes in diffraction peak positions were noted; a slight to a lower angle with an average crystallite size (D) of 20 nm was observed when compared to TiO_2.

The peak at 25.53°might be caused by the overlapping diffraction signals from the TiO_2 and VO_2 crystal phases in the mixed nanostructure [18], as corroborated by the XRD results of the physical mixing of (TiO_2:VO_2) NC_S presented in Table 2.

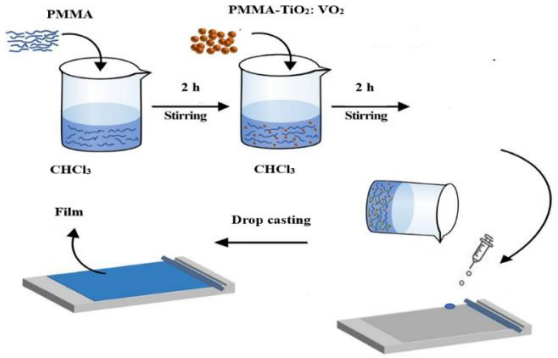

Figure1: Scheme of preparation and synthesis of PMMA-TiO_2;VO_2 thin film used drop casting method.

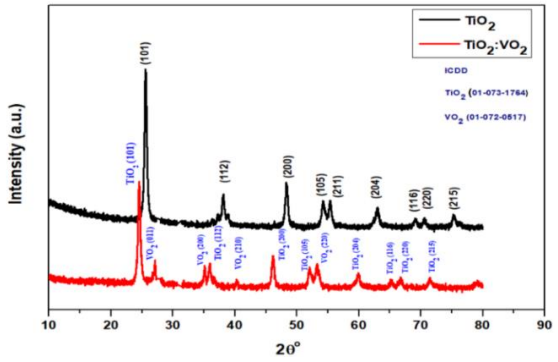

Figure 2: XRD patterns of the (TiO_2 NP_S, TiO_2:VO_2 NC_S).

Table 1: The structural properties of (TiO_2)NP_S.

2θ (deg) Experimental	FWHM (deg)	D (nm)	d_{hkl}(Å) Experimental	hkl
25.58	0.3778	21.55	3.4823	101
38.10	0.3778	22.23	2.3619	112
48.34	0.4723	18.42	1.8828	200
54.18	0.3778	23.60	1.6926	105
55.36	0.3778	23.73	1.6593	211
62.99	0.3778	24.64	1.4756	204
68.99	0.3778	25.52	1.3587	116
70.56	0.3778	25.74	1.3347	220
75.34	0.4723	21.24	1.2614	215
		Dave=22.96 nm		

Table 2: The structural properties of (TiO_2;VO_2)NC_S.

2θ (deg) Experimental	FWHM (deg)	D (nm)	d_{hkl}(Å) Experimental	hkl
25.53	0.4400	19.34	3.4856	101
27.98	0.4164	20.54	3.1811	011
37.21	0.3144	27.85	2.4142	200
38.78	0.4033	21.81	2.3197	112
42.42	0.2982	29.85	2.1289	210
48.25	0.4608	19.73	1.8843	200
54.19	0.5791	16.09	1.6912	105
55.62	0.7753	12.10	1.6574	220
62.86	0.5898	16.49	1.4770	204
68.96	0.5809	17.32	1.3596	116
70.48	0.5625	18.06	1.3348	220
75.27	0.5006	20.93	1.2614	215
		Dave=20nm		

3.2 FTIR Analysis Results

Fourier-transform infrared spectroscopy FTIR analyzed the structural characterization and compatibility of (TiO_2 NP_S, TiO_2:VO_2 NC_S), and PMMA-TiO_2:VO_2 thin film. Figure 3 presents the FTIR spectra of (TiO_2 NP_S, TiO_2:VO_2 NC_S), and PMMA-TiO_2:VO_2 thin film. Altering titanium dioxide TiO_2 may enable the incorporation of hydroxyl (OH) groups and supplementary functional groups. The TiO_2 spectra exhibit an absorption band in the 600–400 cm^{-1} range, attributed to the stretching vibrations of the Ti–O and Ti–O–Ti bonds in TiO_2 [19]. The FTIR spectrum of (TiO_2:VO_2 NCS) has a band at 955.12 cm^{-1}, indicative of the stretching vibrations of the V=O bond, whereas the absorption peak at 585.97 cm^{-1} is associated with bridging oxygen atoms in the V-O-V and Ti-O-Ti bonds. The integrated bridging of V-O-Ti stretching accounts for the IR band at 585.97 [20]. The infrared band at 413

cm^{-1} is ascribed to the stretching vibration of the vanadyl (V–O) bond [21], [22]. The band at around 413 cm^{-1} corresponds to the bending mode of Ti–O [23]. A broad band at 3003 cm^{-1} corresponds to the O–H stretching mode of the hydroxyl group in water. The spectra of PMMA-TiO_2:VO_2 nanocomposites display analogous peaks and additional characteristics, including the vibrational bonds of PMMA. Nevertheless, the presence of pronounced peaks validates the interactions between filler materials and PMMA molecules, while the spectra of PMMA-TiO_2:VO_2 nanocomposites display analogous peaks and other characteristics, including PMMA vibrational linkages. Nevertheless, the presence of pronounced peaks corroborates the interactions between the filler material and PMMA molecules. Peaks at around 1143 cm^{-1} were attributed to C-O-C vibrations. The bands at 2948 cm^{-1} correspond to the vibrational modes of CH_2 and CH_3. The peaks at 1614 and 1722 cm^{-1} correspond to the stretching vibrations of the C=C and C=O functional groups, respectively. Absorption bands within the range of 1435-1382 cm^{-1} were attributed to C-H stretching vibrations [24]. Peaks detected at 3003 cm^{-1} are attributed to surface-adsorbed water and hydroxyl groups [25], [26]. We affirm the incorporation of TiO_2 into the PMMA matrix. Almost all of the peaks of the different samples are identical and resemble pure PMMA. This state arises when PMMA networks entirely and consistently encase the nanostructures without compromising their three-dimensional architecture. Moreover, the stretching vibrations of the polymer group's bands demonstrate increased intensity.

3.3 FESEM Analysis Results

Investigating the surface characteristics of powder (TiO_2 NPs) and composite (TiO_2:VO_2 NCs). The nanoparticle dimensions were calculated with the ImageJ program. The program Origin Pro 8.5 was utilized to illustrate the size distribution and average dimensions of the nanoparticles on the graph. The surface morphology was analyzed via FESEM. The FESEM pictures depict pure TiO_2 nanoparticles, displaying a consistent size distribution and an average diameter of 68.4 nm. Upon mixing with TiO_2:VO_2, the resultant composite nanocrystals exhibit a nearly spherical morphology, with their average size diminishing to 58.6 nm, as illustrated in Figure 4. This outcome is ascribed to the incorporation of VO_2 into titanium dioxide, which can markedly diminish the dimensions of the composite nanocrystals and regulate their morphology [18]. The crystals coalesce to create rounded spherical particles measuring 500 nm. The agglomerated particles combine to create bigger, coarse aggregates, and during mixing, both larger, irregular aggregates and smaller, spherical aggregates are detected [27]. Figure 4a exhibits a scaled image of 500 nm at a magnification of 120,000X. Figure 4b illustrates the diameter distribution of the synthesized nanoparticles. The particles collected were nanoscale in size and exhibited irregular spherical geometries.

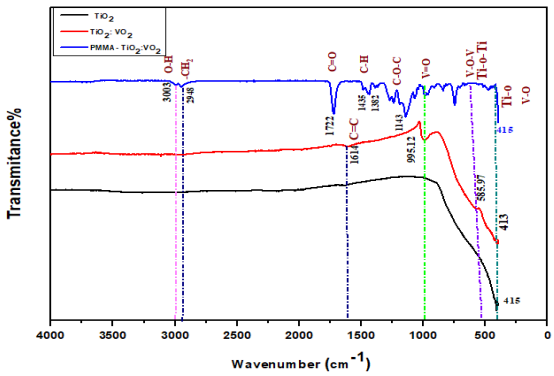

Figure 3: FTIR spectra of (TiO_2 NPs, TiO_2:VO_2 NCs), PMMA- TiO_2:VO_2 thin film.

3.4 EDS Analysis Results

EDS spectra were utilized for the elemental characterization of the chemical components in the manufactured material. The EDS spectra of the produced TiO_2 in the anatase phase are presented in Figure 5a. Titanium (Ti), carbon (C), and oxygen. (O) are the elements present in the anatase phase of titanium dioxide (TiO_2) nanoparticles generated via the sol-gel process. These findings are consistent with study [28]. The proportion of titanium (Ti) in the phase was significantly greater than that of oxygen, as illustrated in the figure. The manifestation of the (C) element results from the influence of the fundamental material ethanol (CH_3CH_2OH) utilized in the synthesis of TiO_2 nanoparticles, as well as from environmental perturbations encountered during the laboratory preparation procedure. Figure 5b illustrates the Energy Dispersive Spectroscopy (EDS) patterns for the mixing process of (TiO_2:VO_2) nanoparticles, indicating that the synthesized samples consist of Titanium (Ti), Oxygen (O), and Vanadium (V) species. The ratios of 62.6%, 25.9%, and 11.5% for Ti, O, and V, respectively, indicate that titanium predominates in vanadium oxide, but a minor quantity of VO_2 may still be incorporated into TiO_2. The EDS spectra indicated the existence of two metal

oxides [29]. The atomic ratio of VO_2 to Ti derived from the EDS measurements aligns well with the composition of the initial material solution. This result signifies that the formulation of the items can be readily regulated and altered as required [30].

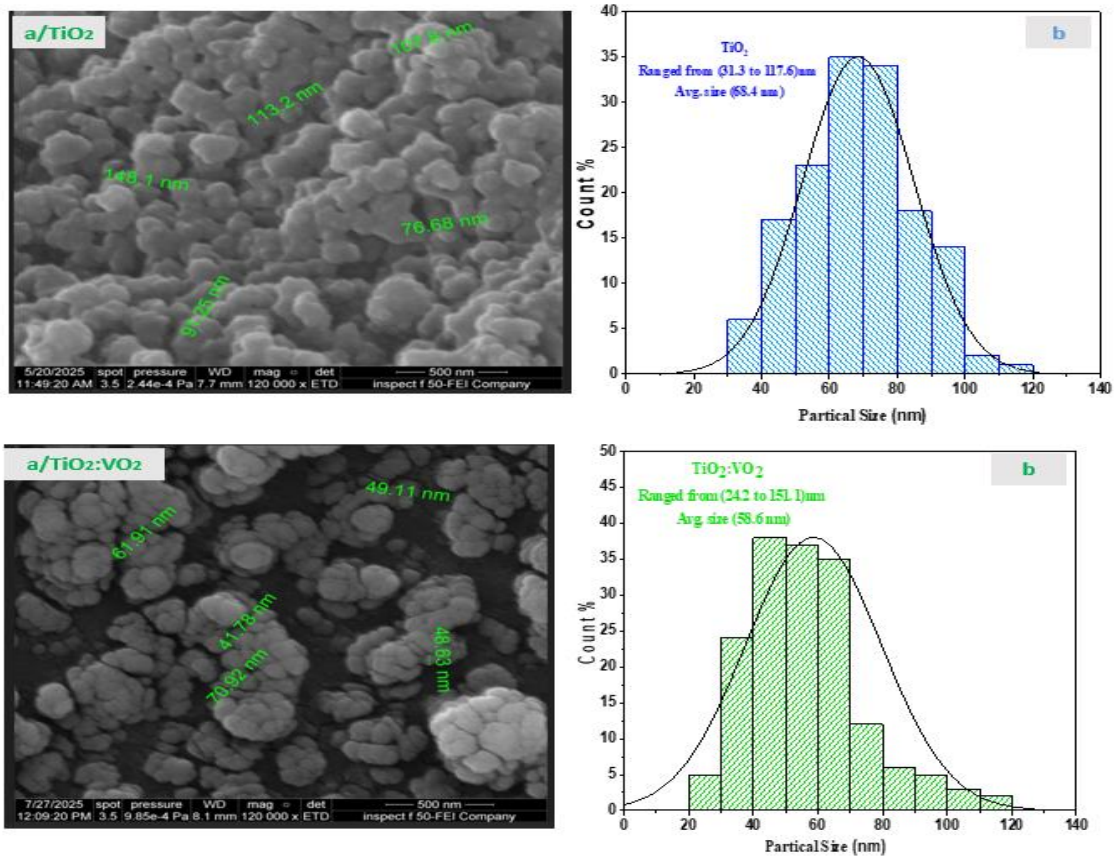

Figure 4: FE-SEM images of (a-TiO_2 NPs, b-TiO_2:VO_2 NCs).

a

Weight %	Atomic %	Element
6.3	16.5	C
16.5	32.5	O
77.2	50.9	Ti

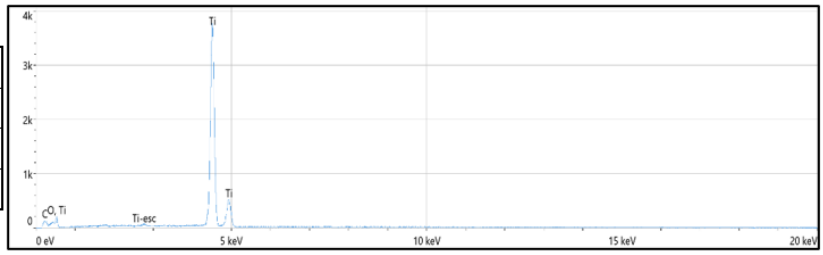

b

Weight %	Atomic %	Element
25.9	51.4	O
62.6	41.4	Ti
11.5	7.2	V

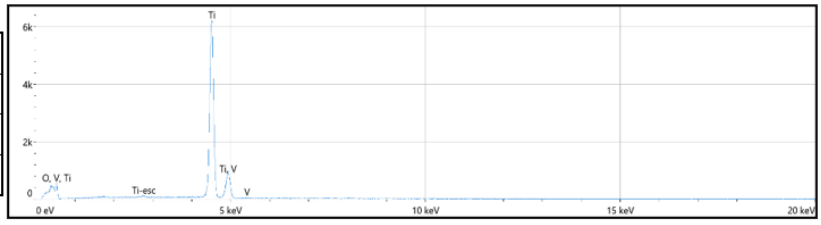

Figure 5: The EDS spectra of (a-TiO_2 NPs, b- TiO_2:VO_2 NCs).

3.5 Optical Properties Results

3.5.1 Absorbance (A)

UV–visible spectroscopy was performed across the wavelength range of 200–900 nm to evaluate the absorbance or transmittance of the produced pure and VO_2 addition TiO_2 nanoparticles. In UV spectroscopic analysis, the shift in TiO_2 and mixed VO_2 is discussed. The shift in the absorbance spectrum following the mixing of VO_2 implies a change in the band gap [31]. Titanium dioxide TiO_2 is a semiconductor with a wide bandgap of 3.25 eV. This indicates that it predominantly absorbs UV light, as photons of more energy (shorter wavelength) than the band gap are required to promote electrons from the valence band to the conduction band. Within the UV spectrum, TiO_2 absorbs light and facilitates the transition of electrons from the valence band to the conduction band. Experimental results indicated that pure TiO_2 exhibits a pronounced absorption peak at 288.27 nm, demonstrating its significant UV absorption capability. Mixing involves the introduction of impurities into a semiconductor material to modify its properties. addition TiO_2 with VO_2 has presumably created additional energy levels inside the band structure VO_2 acts as a donor impurity, supplying additional electrons to the substance. This may induce the emergence of novel energy levels within the band gap of TiO_2. The changing of the material's electronic structure elucidates the alteration in absorbance from ultraviolet to visible wavelengths when TiO_2 is combined with VO_2. The alteration in the spectrum leads to the emergence of an absorption peak at 234.58 nm for the TiO_2–VO_2 sample, accompanied by a notable reduction in absorption intensity, so validating the diminution of the energy gap to approximately 2.75 eV and an enhancement in visible light absorption capacity [32]. The composite films of PMMA-TiO_2:VO_2 exhibit a peak absorption in the ultraviolet (UV) spectrum at around 233.38 nm, attributed to PMMA. The absorbance intensity diminishes further due to the encapsulation of particles within the polymer, which restricts direct interaction between light and the nanoparticles. The incorporation of TiO_2 nanoparticles leads to a diminution in the intensity of the peaks within the visible spectrum, signifying the dominance of TiO_2 characteristics Figure 6. The significant absorption peaks observed in the 200–400 nm range of nanocomposites can be ascribed to the $n \rightarrow \pi^*$ transition, indicating an elevated absorption capacity in these materials [33].

3.5.2 Energy Gap (Eg)

The optical bandgaps of composite materials can be ascertained from the absorption spectra. Absorption is contingent upon electron excitation from the valence band to the conduction band [34]. Thus, the absorption edge defines the material's bandgap. The absorption edge rises with increasing wavelength redshift in the following sequence: (TiO_2 NP_S), (TiO_2:VO_2 NC_S), and PMMA-TiO_2:VO_2 thin film demonstrate a decreasing bandgap in that sequence. The bandgap energy Eg of the composite films was ascertained from the Tauc plot illustrated in Figure7.

$$(\alpha h\upsilon)\, n = B\,(h\upsilon - Eg). \qquad (3)$$

B represents a material-specific constant, hv denotes the photon energy in electron volts (eV), h denotes Planck's constant, v represents the photon frequency, and Eg marks the optical band gap in electron volts (eV). The optical bandgap of TiO_2 is 3.25 eV [35]. A reduction in the energy gap value was noted upon mixing with (TiO_2:VO_2) nanoparticles, resulting in an energy gap value of 2.75 eV. A reduction was noted following vanadium doping. The reduction in bandgap values noted for the V-doped TiO_2 This phenomenon is due to charge transfer between the conduction (or valence) band of TiO_2 and the d electrons of the vanadium dopant [36]. Figure 7 demonstrates this. The energy gap values are contingent upon the crystal structure of the composites and the configuration and distribution of atoms within the crystal lattice; hence, a reduction in the energy gap is associated with an increase in disorder within the material [37]. However, during the mixing of the composite, defects such as voids may form, leading to the emergence of favorable localized states inside the material's band gap, as well as a reduction in the cluster size of the parent solution [38]. The energy gap of the (PMMA-TiO_2:VO_2) film decreased to 2.35 eV in comparison to the pure TiO_2 film, a phenomenon attributed to enhanced ion transport within the constituents of the PMMA-TiO_2:VO_2 nanocomposite thin films [39].

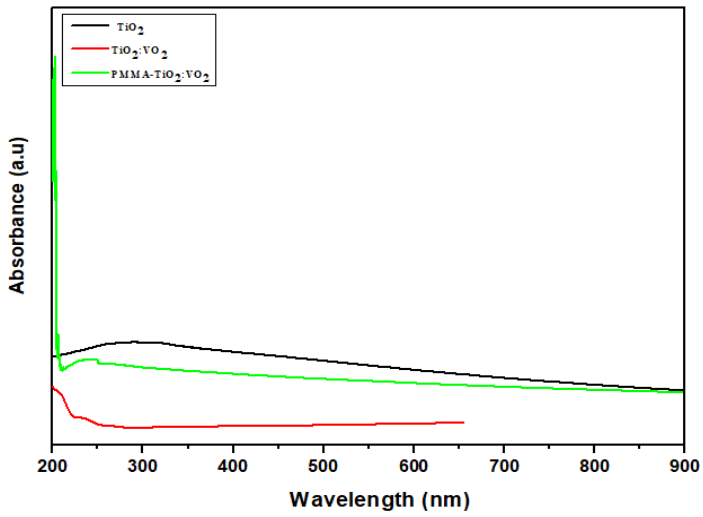

Figure 6: Absorbance spectra of (TiO_2 NPs, TiO_2:VO_2 NCs), PMMA- TiO_2:VO_2 thin film.

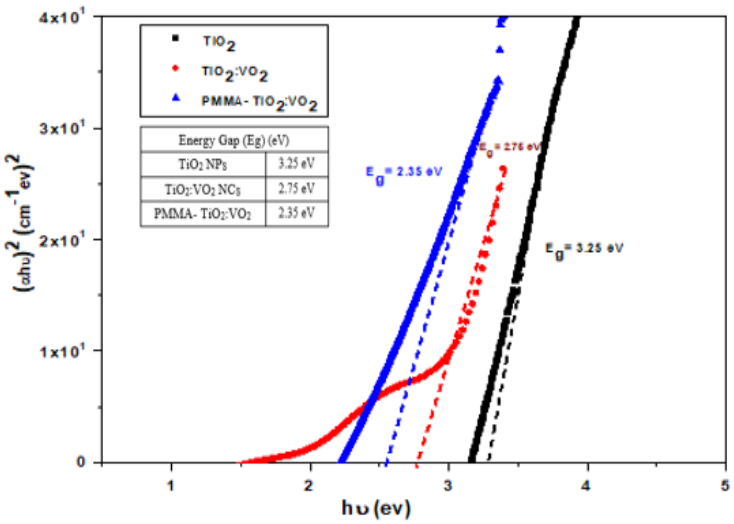

Figure 7: Tauc's plot of (TiO_2 NPs, TiO_2:VO_2 NCs), PMMA- TiO_2:VO_2 thin film.

4 CONCLUSIONS

Titanium oxide TiO_2 was effectively synthesized via the sol-gel process, exhibiting a well-ordered anatase crystalline phase with nanoscale crystal dimensions and pronounced optical characteristics in the ultraviolet region. The introduction of VO_2 resulted in a slight shift in the diffraction peaks and a significant the interaction between titanium oxide and vanadium oxide results in a reduction of the energy gap from 3.25 eV to 2.75 eV, signifying enhanced absorption in the visible light spectrum. The introduction of the TiO_2:VO_2 mixture within the PMMA polymer resulted in the formation of a homogeneous nanofilm that exhibited distinct bonds in the FTIR spectra, The process involves verifying the interaction between the polymer and the nanocomposites, which is accompanied by a subsequent reduction in the energy gap of roughly 2.35eV. FESEM images revealed pure TiO_2 nanoparticles with an average diameter of around 68.4 nm and a consistent size distribution. The addition of VO_2 led to the development of smaller spherical crystals averaging 58.6 nm, with larger spherical aggregates (about 500 nm) and irregular clusters.The results show that adding TiO_2 and VO_2 to the PMMA matrix improves the material's optical and structural properties, making it an effective candidate for smart window and self-cleaning membrane applications.

ACKNOWLEDGMENTS

The authors would like to express their sincere gratitude to the Department of Physics, College of Science, University of Diyala, for their continuous support and provision of the necessary facilities to conduct this research. The authors also extend their appreciation to all colleagues and technical staff whose guidance and assistance contributed to the successful completion of this study.

REFERENCES

[1] M. C. Daniel and D. Astruc, "Gold nanoparticles: assembly, supramolecular chemistry, quantum-size-related properties, and applications toward biology, catalysis, and nanotechnology," Chem. Rev., vol. 104, no. 1, pp. 293-346, 2004, [Online]. Available: https://doi.org/10.1021/cr030698+.

[2] A. N. Shipway, E. Katz, and I. Willner, "Nanoparticle arrays on surfaces for electronic, optical, and sensor applications," ChemPhysChem, vol. 1, no. 1, pp. 18-52, 2000, [Online]. Available: https://doi.org/10.1002/1439-7641(20000804)1:1<18::AID-CPHC18>3.3.CO;2-C.

[3] M. P. Stevens, Polymer Chemistry: An Introduction, 3rd ed. New York, NY, USA: Oxford Univ. Press, 1999, pp. 167-176, 256-276.

[4] A. K. Gupta, M. Bafna, and Y. K. Vijay, "Study of optical properties of potassium permanganate ($KMnO_4$) doped poly(methyl methacrylate) (PMMA) composite films," Bull. Mater. Sci., vol. 41, p. 160, 2018, [Online]. Available: https://doi.org/10.1007/s12034-018-1606-4.

[5] U. Ali, K. J. B. A. Karim, and N. A. Buang, "A review of the properties and applications of poly(methyl methacrylate) (PMMA)," Polym. Rev., vol. 55, pp. 678-705, 2015, [Online]. Available: https://doi.org/10.1080/15583724.2014.971124.

[6] C. Chang, S. Rad, L. Gan, Z. Li, J. Dai, and A. Shahab, "Review of the sol–gel method in preparing nano TiO_2 for advanced oxidation process," Nanotechnol. Rev., vol. 12, no. 1, pp. 530-539, 2023, [Online]. Available: https://doi.org/10.1515/ntrev-2023-0035.

[7] A. Md Alamgir, G. C. Mallick, S. K. Nayak, and S. Tiwari, "Development of PMMA/TiO_2 nanocomposites as excellent dental materials," J. Mater. Sci. Technol., vol. 33, no. 10, pp. 4755-4760, 2019, [Online]. Available: https://doi.org/10.1016/j.jmst.2019.07.009.

[8] G. A. Niklasson, S.-Y. Li, and C.-G. Granqvist, "Thermochromic vanadium oxide thin films: electronic and optical properties," J. Phys.: Conf. Ser., vol. 559, no. 1, p. 012001, 2014, [Online]. Available: https://doi.org/10.1088/1742-6596/559/1/012001.

[9] M. Taha, A. Al-Khafaji, A. Al-Azzawi, and H. Al-Mashhadani, "Insulator–metal transition in substrate-independent VO_2 thin film for phase change devices," Sci. Rep., vol. 7, no. 1, p. 17899, 2017, [Online]. Available: https://doi.org/10.1038/s41598-017-18277-8.

[10] X.-J. Huang, X.-F. Zeng, J.-X. Wang, and J.-F. Chen, "Transparent dispersions of monodispersed ZnO nanoparticles with ultrahigh content and stability for polymer nanocomposite film with excellent optical properties," Ind. Eng. Chem. Res., vol. 57, no. 12, pp. 4253-4260, 2018, [Online]. Available: https://doi.org/10.1021/acs.iecr.7b05392.

[11] M. A. Haruna and D. Wen, "Stabilization of polymer nanocomposites in high-temperature and high-salinity brines," ACS Omega, vol. 4, no. 7, pp. 11631-11641, 2019, [Online]. Available: https://doi.org/10.1021/acsomega.9b01234.

[12] Y. Ke, J. Zhang, Q. Wang, Y. Liu, and H. Wang, "Adaptive thermochromic windows from active plasmonic elastomers," Joule, vol. 3, no. 3, pp. 858-871, 2019, [Online]. Available: https://doi.org/10.1016/j.joule.2018.12.018.

[13] Y. Zhou, Y. Cai, X. Hu, and Y. Long, "VO_2/hydrogel hybrid nanothermochromic material with ultra-high solar modulation and luminous transmission," J. Mater. Chem. A, vol. 3, no. 3, pp. 1121-1126, 2015, [Online]. Available: https://doi.org/10.1039/C4TA05692A.

[14] R. J. Deokate, S. S. Mali, C. D. Lokhande, and P. S. Patil, "Structural and optical properties of spray-deposited Cu_2ZnSnS_4 thin films," Energy Procedia, vol. 54, pp. 627-633, 2014, [Online]. Available: https://doi.org/10.1016/j.egypro.2014.07.314.

[15] L. Kernazhitsky, A. Sakhatsky, V. Strelchuk, and V. Sklyar, "Optical absorption of polydisperse TiO_2: effect of surface doping by transition metal cations," Ukr. J. Phys. Opt., vol. 14, no. 1, pp. 15-23, 2013.

[16] M. Yaghmaei, A. R. Moradi, M. R. Ganjali, and P. Norouzi, "Innovative black TiO_2 photocatalyst for effective water remediation under visible light illumination using flow systems," Catalysts, vol. 14, no. 11, p. 775, 2024, [Online]. Available: https://doi.org/10.3390/catal14110775.

[17] K. Thamaphat, P. Limsuwan, and B. Ngotawornchai, "Phase characterization of TiO_2 powder by XRD and TEM," Kasetsart J. Nat. Sci., vol. 42, no. 5, pp. 357-361, 2008.

[18] D. Li, Y. Wang, J. Liu, and H. Zhang, "Hydrothermal synthesis of Mo-doped VO_2/TiO_2 composite nanocrystals with enhanced thermochromic performance," ACS Appl. Mater. Interfaces, vol. 6, no. 9, pp. 6555-6561, 2014, [Online]. Available: https://doi.org/10.1021/am501274w.

[19] T. A. M. Msagati and J. F. Nure, "Optimization of photocatalytic degradation of Eriochrome Black T from aqueous solution using TiO_2-biochar composite," Results Eng., vol. 25, p. 104036, 2025, [Online]. Available: https://doi.org/10.1016/j.reng.2025.104036.

[20] E. M. Mostafa and E. Amdeha, "Enhanced photocatalytic degradation of malachite green dye by highly stable visible-light-responsive Fe-based tri-composite photocatalysts," Environ. Sci. Pollut. Res., vol. 29, no. 43, pp. 69861-69874, 2022, [Online]. Available: https://doi.org/10.1007/s11356-022-22125-7.

[21] M. A. Awad, A. M. El-Kady, M. A. El-Sayed, and A. M. El-Shazly, "Wet chemical synthesis and characterization of $FeVO_4$ nanoparticles for supercapacitor as energy storage device," J. King Saud Univ.–Sci., vol. 35, no. 4, p. 102857, 2023, [Online].

Available: https://doi.org/10.1016/j.jksus.2023.102857.

[22] E. M. Mostafa, R. M. El-Sherif, E. S. Noemy, and R. E. Hammam, "Evaluation of stability, optical properties, and thermal performance of innovative $TiO_2/FeVO_4$ ethylene glycol hybrid nanofluids," Environ. Sci. Pollut. Res., vol. 31, no. 1, pp. 112-125, 2025, [Online]. Available: https://doi.org/10.1007/s11356-024-32567-9.

[23] L. S. Chougala, S. S. Mali, C. D. Lokhande, and P. S. Patil, "A simple approach on synthesis of TiO_2 nanoparticles and its application in dye sensitized solar cells," J. Nano Electron. Phys., vol. 9, no. 4, p. 4001, 2017.

[24] S. Dalla Bernardina, M. S. Dresselhaus, and G. Dresselhaus, "Water in carbon nanotubes: the peculiar hydrogen bond network revealed by infrared spectroscopy," J. Am. Chem. Soc., vol. 138, no. 33, pp. 10437-10443, 2016, [Online]. Available: https://doi.org/10.1021/jacs.6b05873.

[25] H. Yuwono, C. S. Lim, and J. Wei, "Controlling the crystallinity and nonlinear optical properties of transparent TiO_2–PMMA nanohybrids," J. Mater. Chem., vol. 14, no. 20, pp. 2978-2987, 2004, [Online]. Available: https://doi.org/10.1039/B403944A.

[26] S. Borandeh, A. Abdolmaleki, S. Z. Nekuabadi, and M. Sadeghi, "Methoxy poly(ethylene glycol) methacrylate–TiO_2/poly(methyl methacrylate) nanocomposite: an efficient membrane for gas separation," Polym.-Plast. Technol. Mater., vol. 58, no. 8, pp. 789-802, 2019, [Online]. Available: https://doi.org/10.1080/03602559.2018.1556670.

[27] N. Khatun, M. A. Gaffar, M. A. Islam, and M. A. Hossain, "Effect of lattice distortion on band gap decrement due to vanadium substitution in TiO_2 nanoparticles," Mater. Sci. Semicond. Process., vol. 50, pp. 7-13, 2016, [Online]. Available: https://doi.org/10.1016/j.mssp.2016.03.006.

[28] J. M. Selvi, R. S. Rajkumar, and S. R. Kumar, "Green synthesis, characterization and applications of TiO_2 nanoparticles using aqueous extract of Erythrina variegata leaves," Curr. Sci., vol. 123, no. 1, pp. 59-66, 2022, [Online]. Available: https://doi.org/10.18520/cs/v123/i1/59-66.

[29] R. V. S. S. N. Ravikumar, K. V. Ramesh, and K. S. R. Anjaneyulu, "Spectral investigation of structural and optical properties of mechanically synthesized TiO_2–V_2O_5 nanocomposite powders," Mater. Today: Proc., vol. 3, no. 1, pp. 31-38, 2016, [Online]. Available: https://doi.org/10.1016/j.matpr.2016.01.005.

[30] C. Hu, H. Xu, X. Liu, F. Zou, L. Qie, Y. Huang, and X. Hu, "VO_2/TiO_2 nanosponges as binder-free electrodes for high-performance supercapacitors," Sci. Rep., vol. 5, p. 16012, 2015, [Online]. Available: https://doi.org/10.1038/srep16012.

[31] Y. E. Tasisa, T. K. Sarma, R. Krishnaraj, and S. Sarma, "Band gap engineering of titanium dioxide (TiO_2) nanoparticles prepared via green route and its visible light driven for environmental remediation," Results Chem., vol. 11, p. 101850, 2024, [Online]. Available: https://doi.org/10.1016/j.rechem.2024.101850.

[32] U. J. R. Babu, K. Hareesh, S. R. Rondiya, D. H. Nagaraju, and K. Mahendra, "Synthesis and characterization of nitrogen and phosphorus co-doped TiO_2 nanoparticle anchored graphitic carbon nitride nanosheets: photocatalytic application on dye removal," Diam. Relat. Mater., vol. 139, p. 110292, 2023, [Online]. Available: https://doi.org/10.1016/j.diamond.2023.110292.

[33] V. S. Bhat, S. B. Kapatkar, I. Naik, and S. Hegde, "Optical, electrical, structural properties of PFO–PMMA films loaded with TiO_2 nanoparticles," Discov. Mater., vol. 4, no. 1, p. 50, 2024, [Online]. Available: https://doi.org/10.1007/s43939-024-00050-9.

[34] K. Omri and F. Alharbi, "Synthesis and effect of temperature on morphological and photoluminescence properties of TiO_2 nanoparticles," Appl. Phys. A, vol. 125, no. 10, p. 696, 2019, [Online]. Available: https://doi.org/10.1007/s00339-019-2969-6.

[35] E. M. Taha and N. A. Abdulrahman, "Characteristics and synthesis of TiO_2 and B-TiO_2 by solvothermal method," J. Nanostruct., vol. 14, no. 1, pp. 109-115, 2024, [Online]. Available: https://doi.org/10.22052/JNS.2024.01.013.

[36] O. Sacco, D. Sannino, M. Matarangolo, and V. Vaiano, "Room temperature synthesis of V-doped TiO_2 and its photocatalytic activity in the removal of caffeine under UV irradiation," Materials, vol. 12, no. 6, p. 911, 2019, [Online]. Available: https://doi.org/10.3390/ma12060911.

[37] C. Rameshkumar, S. Sarojini, K. Naresh, and R. Subalakshmi, "Preparation and characterization of pristine PMMA and PVDF thin film using solution casting process for optoelectronic devices," J. Surf. Sci. Technol., vol. 33, no. 1-2, pp. 12-18, 2017.

[38] Q. Al-Bataineh, A. Ahmad, and A. Alsaad, and A. Telfah, "Optical characterizations of PMMA/metal oxide nanoparticles thin films: bandgap engineering using a novel derived model," Heliyon, vol. 7, no. 4, p. e05952, 2021, [Online]. Available: https://doi.org/10.1016/j.heliyon.2021.e05952.

[39] S. Al-Khafaj, K. A. Jasim, and A. M. Ibraheim, "Optical and thermal characterizations of PMMA composites," Eng. Technol. J., vol. 37, no. B2, pp. 20-27, 2019.